RSC Advances

ROYAL SOCIETY OF CHEMISTRY

www.rsc.org/advances

RSC Advances

PAPER

Nonlinear optical effects in nitrogen–doped graphene

Fang Zhang[a, b], Zhengping Wang[a, b, †], Duanliang Wang[a, b], Zhixin Wu[a, b], Shenglai Wang[a, b], Xinguang Xu[a, b]

Received 00th January 20xx,
Accepted 00th January 20xx

DOI: 10.1039/x0xx00000x

www.rsc.org/

The band structure of graphene can be adjusted by incorporating other elements or functional groups, correspondingly the response to external light field will also be changed. In this paper, we researched the nonlinear optical (NLO) responses of N-doped graphene nanosheets (N-Gns) with open aperture Z-scan method, under the excitation of pico-second laser pulses. As we have known, this is the first time that the two-photon absorption (2PA) of N-Gns was reported. The normalized nonlinear transmission demonstrates that with the increasing of excitation energy the saturable absorption (SA) and the 2PA appear successively. Compared to the 532 nm excitation, the 1064 nm excitation exhibits smaller saturable intensity I_s and larger 2PA coefficient β. At the same time, the N-Gns present superior NLO property compared to the pure graphene. Consequently, N-Gns will be a promising candidate for SA or optical limiting (OL) applications.

Introduction

Owing to the rare and precious properties, such as high optical transparency, flexible mobility, excellent elongation and thermal conductivity[1-5], graphene opened a new nano-world since it was first exfoliated from graphite in 2004[6]. Strong intra-layer covalent bonding and weak inter-layer van der Waals interaction allow graphene to form a tough two-dimensional (2D) nanostructure. Due to the unique band structure where the conduction band and the valance band meet at the Dirac point, carbon-based graphene exhibits a number of remarkable optoelectronic properties, which have potential applications in electronics, optics, magnetic, biomedicine, energy storage and other domains. In the past, a large number of works have devoted to the electronic properties of graphene[3, 5, 6-9], until recent several years people began to pay attention to the optical properties of graphene[1, 9], particularly, the NLO characteristics of graphene[10-14]. The SA[13, 14] and OL effects[11, 12] over a broad waveband (from visible to infrared) have been found in graphene. The SA is the consequence of Pauli Exclusion Principle. When the excitation energy reaches to the saturation intensity, the photo-excited carriers are saturated and the remaining excitation photons can transparently transmitted, i.e. these photons will not be absorbed. Utilizing this property, graphene can serve as the passively saturable absorber in Q-switched or mode-locked lasers[15, 16]. The mechanism of OL effect comes from reverse saturable absorption (RSA), multi-photon absorption, and free-carrier absorption (FCA). Utilizing the OL effect of graphene, new laser protecting technology for sensitive optical components and human eyes can be developed in the future.

Nevertheless, the intrinsic zero band gap structure[4-6] of graphene brings many limitations for electronic and photonic applications. Doping is an effective method to adjust the band gap and tailor the optoelectronic properties of graphene. Recently, some doped graphenes such as graphene-polymer[17], graphene/ZnO[18], NH_4 functionalized graphene[19], graphene-porphyrin composites[20] have been reported successively. In 2009, the N-Gns were firstly synthesized by chemical vapor deposition (CVD) method[21]. The doping of N atoms opens the intrinsic zero band gap structure of graphene and leads to a semiconductor like transition, which greatly expands the applications. In this paper, the NLO properties of N-Gns were researched by the Z-scan technique of pico-second pulse lasers. For the first time the OL behavior of N-Gns was observed. The results indicate that N-Gns is an excellent NLO material for SA and OL applications.

Characterization

The original powder was brought from Nanjing XFNANO Materials Tech Co. Ltd. of China. It was synthesized by the CVD method[21-23], based on the oxidation-reduction reaction of graphene oxide and ammonia gas. The electrical conductivity was over 1000 S/m, and the nitrogen content was 3.0-5.0 at.%. To detect the size and the thickness of N-Gns, an atomic force microscopy (AFM) measurement was carried out. The appropriate powder was dissolved in ultrapure water. In order to enhance the dissolution of the sample, surfactant Polyvinylpyrrolidone (PVP) was added with eight times content of the N-Gns. After ultrasound treatment of two hours at a power of 300 W, the dispersion liquid was prepared completely. A part of the dispersion liquid was stored in a quartz colorimetric utensil of 2 mm thickness for NLO experiment. The rest part was dropped on a pre-cleaned quartz substrate, and placed in a vacuum device at room temperature to get rid of the residual

[a] State Key Laboratory of Crystal Materials, Shandong University, Jinan 250100, China.
[b] Key Laboratory of Functional Crystal Materials and Device, Shandong University, Ministry of Education, Jinan 250100, China.
† Corresponding author: zpwang@sdu.edu.cn. Fax: +86 53188364848; Tel: +86 53188364848

solvent, as the sample of basic properties measurement. Figure 1 shows the AFM image (left) and the thickness profiles (right) of the representative deposited N-Gns. The results reveal that most of the N-Gns have the radial dimension of a few hundred nanometers. About 80% of the N-Gns have the thicknesses of 5 nm or so. Considering the aggregation effect during the preparing process of AFM sample including deposition and drying, the actual thicknesses of N-Gns in dispersion might be less than 5 nm, which indicates that the powder consists of 1~5 atomic layer graphene nanosheets.

The result of X-ray photoelectron spectroscopy (XPS) confirms the doping of nitrogen, as shown in figure 2. The concentration of nitrogen was calculated to be 1.6 at.%. In the manufacturing process, some oxygen element was remained in the sample which was 7.0~7.5 at.% due to the incomplete reduction reaction, so the O 1s peak around 532.0 eV was observed (Figure 2a). The other peaks at 284.7 and 399.5 eV derived from C 1s of sp^2 C and N 1s of the doped N, respectively. The N 1s peak (Figure 2b) consists of three peaks, which indicates that the N atoms exist in graphene in the way of three different bonding structures. According to the reference[21], the peaks at 398.2 and 399.5 eV originate from the π conjugated system of N atoms and the difference is the number of

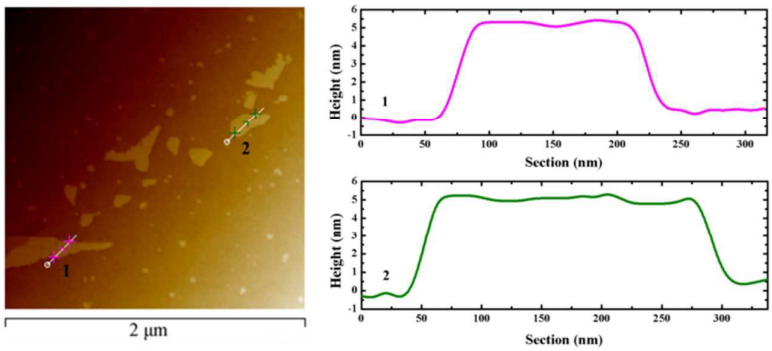

Figure 1 Typical AFM image (left) and thickness profiles (right).

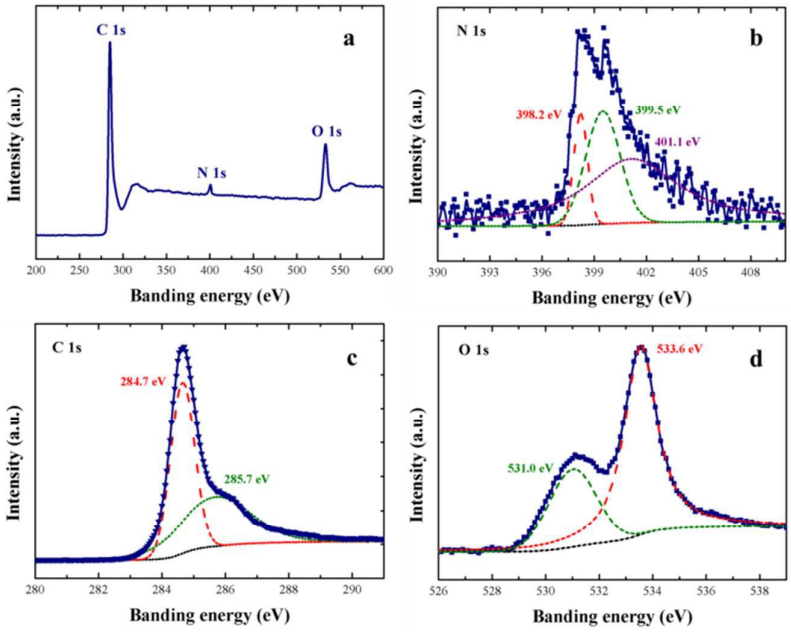

Figure 2 (a) XPS result of N-Gns. (b) N 1s spectrum, (c) C 1s spectrum, (d) O 1s spectrum. The N 1s peak can be split to three Lorentzian peaks at 398.2, 399.5 and 401.1 eV, which are labeled by red, green, and purple dashed lines. The C 1s peak can be split to two Lorentzian peaks at 284.7 and 285.7 eV, which are labeled by red and green dashed lines. The O 1s peak can be split to two Lorentzian peaks at 531.0 and 533.6 eV, which are labeled by green and red dashed lines.

RSC Advances

ARTICLE

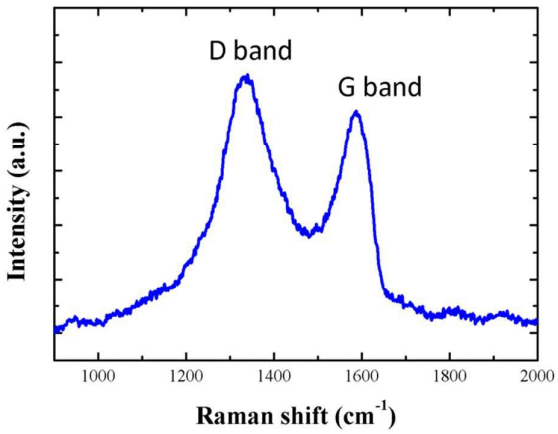

Figure 3 Raman spectrum of the N-doped graphene.

p-electrons (corresponding to one and two p-electrons, respectively) contributed to the π system. The peak at 401.1 eV comes from the substitution of honeycomb C atoms in graphene. The C 1s spectrum (Figure 2c) is composed of two Lorentzian peaks. The stronger peak at 284.7 eV corresponds to the sp^2 C-C band itself, which reflects the honeycomb lattice structure of the pure graphene. The peak at 285.7 corresponds to the sp^2 C-N, which originates from the substitution of N atoms or the defects of the N-Gns. As shown in Figure 2d, the O 1s peak can be split into two Lorentzian peaks. The stronger peak at 533.6 eV comes from the sp^2 C-O bond and the weaker peak at 531.0 eV dues to the combined actions of C=O, O-C=O and O-CO-O bonds[24].

The Raman spectrum of N-doped graphene was shown in figure 3, which was much similar to those reported by Anand et al.[25] The N doping creates a large amount of topological defects, and the sp^2 C of these defects induces the much stronger D band Raman peak at ~1330 cm^{-1}, on the contrary for the pure graphene this peak is very faint.[25] So the obvious D band Raman peak in Fig. 3 reflects the effective N doping and the increasing of lattice disorder. The G band Raman peak is at 1584 cm^{-1}, which is identical to the pure graphene.

NLO experiment

The open aperture Z-scan technique was used to investigate the NLO properties of the as-prepared N-Gns dispersion liquid. As mentioned above, appropriate surfactant PVP was added to enhance the dissolution of the sample. The dispersion was stored in a quartz colorimetric utensil with 2 mm thickness. Figure 4 displays the experimental setup with 1064 and 532 nm laser excitations. The laser resource was a dye mode-locked Nd:YAG laser operating at 1064 nm, 40 ps pulses, with 10 Hz repetition rate. A KTP crystal was used to generate the frequency doubling laser of 532 nm with a pulse width of 30 ps. The flat mirror M_1 served as the filter of the fundamental laser, which was highly transmitted at 532 nm (T>80%) and highly reflective at 1064 nm (R>99.5%). The focal length of the convex lens is 30 cm.

Figure 5 was the measurement results for 1064 and 532 nm excitations. The sample exhibited SA behavior (single photon absorption) when the excitation energy was weak. Under high excitation energy, with the increasing of excitation intensity, the single photon absorption (1PA) became saturated and the two photon absorption (2PA) followed behind. When the excitation energy increased further, the OL effect became more significant. In Z-scan experiment, the reducing of normalized linear transmittance which was induced by OL effect could be defined as “OL depth”. Thus, the OL depths were 32% at 1064 nm, 6 μJ excitation, and 63% at 532 nm, 12 μJ excitation, as shown in figure 5. The SA threshold at 1064 nm excitation was 4.1 mJ/cm^2, which was much lower than the value at 532 nm excitation (8.5 mJ/cm^2). The relatively weaker SA threshold indicates the superiority as saturable absorber at infrared waveband. As the reference, no NLO effects were observed from the PVP water solution without N-Gns.

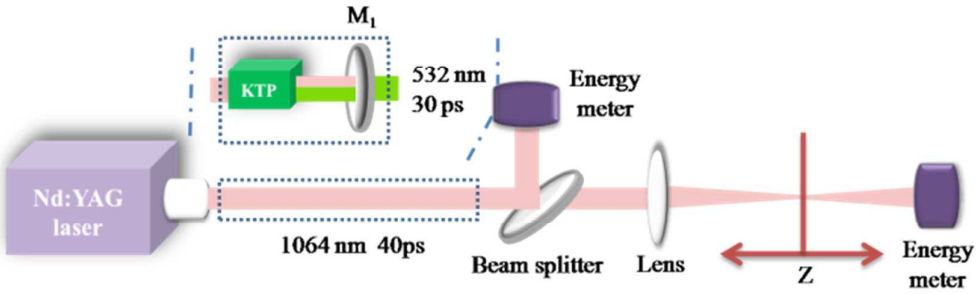

Figure 4 Open-aperture Z-scan experimental setup with 1064 and 532 nm laser excitations.

RSC Advances

ARTICLE

The inserts of Figure 5 display the schematic diagrams for the energy level transitions of 1PA and 2PA in N-Gns. The SA effect is the consequence of 1PA process. Under the excitation of external laser, the electrons jump to the conduction band from the valence band, and subsequently cooled down in the constraint of the Pauli Exclusion Principle. When the incident intensity reaches the saturation intensity, the photo-carrier intensity is saturated and the remaining photons will transparently pass through, i.e. these photons will not be absorbed. As shown in the inserts of Figure 5, to achieve the SA effect, the long-wavelength photon excitation requires a lower intensity to fully fill the lower energy levels compared to a short-wavelength photon excitation. When the excitation energy is increased further, two excitation photons tangle together and the electrons are stimulated into much higher energy levels. Accordingly, the transmittance declined rapidly. From the inserts of Figure 5, it can be seen that for 2PA the long wavelength excitation of 1064 nm corresponds to smaller energy band volume, compared to the short wavelength excitation of 532 nm. It means that the 2PA of 1064 nm excitation corresponds to fewer energy levels, i.e. fewer absorbed photon numbers. The small single photon energy and few absorbed photon numbers lead that the 2PA threshold of 1064 nm excitation is obviously lower than that of 532 nm excitation, at the same time the 2PA adjusting depth of 1064 nm excitation is smaller, which agree to the experimental results demonstrated in figure 6. From this figure it can be seen that for each excitation there are three different NLO stages. For 1064 nm excitation (figure 6a), when the excitation energy varies from 4.1 to 12.6 mJ/cm^2, the SA is the dominated NLO effect. When the excitation energy is in the range of 12.6 – 33.9 mJ/cm^2, the SA and the OL effects co-exist. When the excitation energy exceeds 33.9 mJ/cm^2, the OL behavior becomes the main NLO effect. For 532 nm excitation, these three stages correspond to the excitation energy of less than 34.0 mJ/cm^2, in the range of 34.0 – 69.8 mJ/cm^2, and beyond 69.8 mJ/cm^2, respectively (Figure 6b). In Fig. 6, we used the transmittance variation of 1% as the distinguishing criteria of different stages. When the transmittance increased to 101% of the starting linear transmittance value 1 and hereafter continued to increase, we set the corresponding energy fluence as the SA threshold. When the transmittance decreased to 99% of the highest transmittance, the corresponding interval range of energy fluence was set as the coexistence region of SA and OL. And then the SA region and OL region could be determined. The experimental results illustrate that by appropriately controlling the laser energy density N-Gns can be selected to be the SA material or the OL material. The former can be used in passively mode-locking and Q-switching, and the latter can be used to protect human eyes or sensitive optical components from laser-induced damage.

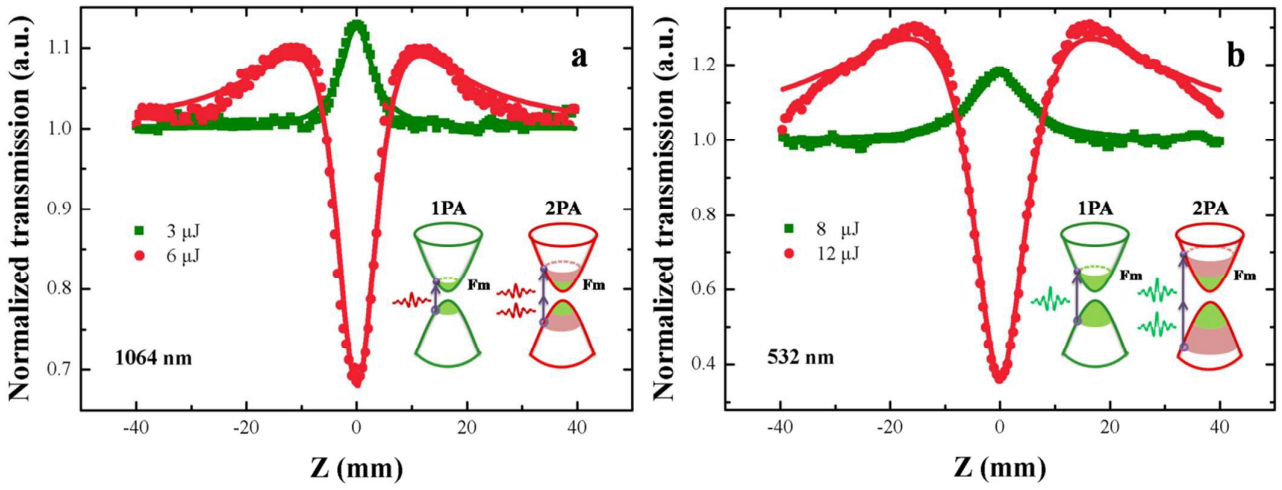

Figure 5 Open-aperture Z-scan results of N-Gns dispersion with excitation wavelength at (a) 1064 and (b) 532 nm. (The discrete points are experimental data, and the solid lines are the fitted curves). Inserts: schematic diagrams for the energy level transitions of 1PA and 2PA in N-Gns.

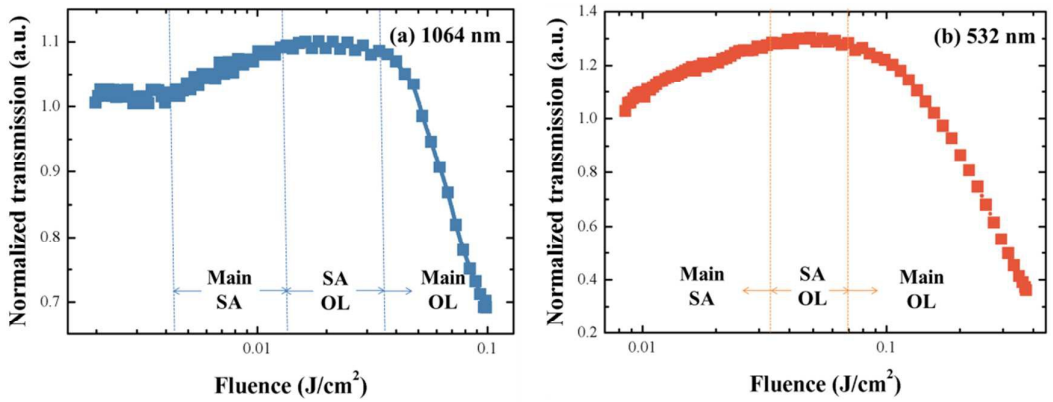

Figure 6 Three different NLO stages including SA and OL behaviors with excitation at (a) 1064 and (b) 532nm.

Discussion.

The normalized transmittance in the Z-scan measurement can be expressed by equation 1, where α and α_0 are the total and linear absorption, respectively, and l is the sample length. The same linear absorption coefficient α_0 of 2.23 cm^{-1} was measured for both of 1064 and 532 nm. The excitation intensity $I(z)$ is determined by the peak intensity I_0 at z = 0, the Rayleigh length z_0 of the beam and the position z of the sample (equation 2). For a system in which SA and 2PA co-exist[17, 26], the total absorption $\alpha(I)$ can be described by equation 3, where β is the 2PA coefficient and I_s is the saturable intensity, defined as the optical intensity when the optical absorbance is reduced to one half of its unbleached value. The first and the second terms on the right side of equation 3 represent the SA and the 2PA, respectively. Combining with equations 1-3, the normalized transmittance can be expressed as equation 4, which is used to fit the Z-scan experimental data.

$$T = (1-\alpha l)/(1-\alpha_0 l) \quad (1)$$

$$I(z) = I_0/(1+z^2/z_0^2) \quad (2)$$

$$\alpha(I) = \frac{\alpha_0}{1+I/I_s} + \beta I \quad (3)$$

$$T = [1 - \frac{\alpha_0 I_s l}{I_s + I_0/(1+z^2/z_0^2)} - \beta I_0 l/(1+z^2/z_0^2)]/(1-\alpha_0 l) \quad (4)$$

The theoretical fitting curves were plotted in figure 5 along with the experimental points. It can be seen that they present perfect agreements. For 1064 nm excitation, the saturable intensity I_s and the 2PA coefficient β are fitted to be 0.35 GW/cm^2 and 0.76 cm/GW, respectively. For 532 nm excitation, I_s and β are fitted to be 0.87 GW/cm^2 and 0.46 cm/GW, respectively. The lower I_s at 1064 nm excitation indicates that long wavelength laser (such as infrared light) can easily realize the SA in N-Gns, which can be used in passively mode-locked lasers. This property is hopeful to change the current research situation of solid-state lasers, i.e. the infrared laser (particularly the far infrared laser) is difficult to reach high energy output[27, 28]. At the same time, the 2PA coefficient β of N-Gns changes larger as the wavelength increases, which implies excellent sensitivity and good OL effect for infrared laser. In many previous literatures on two-dimensional materials, the β at 1064 nm is often smaller than that at 532 nm. While there were also some contrary examples which were consistent with the present result, such as functionalized multilayer graphene (fG)[29], graphene nanoribbons (GNRs) and graphene oxide nanoribbons (GONRs)[12]. We speculate that the relative magnitude of β at different wavelengths will be related to the content of N. As introduced at the beginning of the "Characterization" part, we only have one kind of N-Gns sample at hand. Maybe in the future more abundant results about β at different wavelengths could be obtained, when more samples with different N contents are available.

For 1064 and 532 nm excitations, the absorption cross-section σ ($\sigma = \hbar\omega\beta/N_0$, where $\hbar\omega$ is the excitation photon energy and $N_0 \approx 5\times10^{16}$ cm^{-3} is the density of N-Gns sample in the ultrapure water) are calculated to be 2.8×10^{-45} and 3.4×10^{-45} $cm^4 \cdot s \cdot photon^{-1}$. They are comparable to the value of double-decker $Pr[Pc(OC_8H_{17})_8]_2$ rare earth complex[30]. In addition, we measured nonlinear transmission of the pure graphene under the same experimental conditions. For 1064 and 532 nm excitations, the N-Gns has exhibited stronger NLO effects, as shown in Figure 7. Under the present experimental conditions, we didn't observed obvious SA phenomenon from pure graphene. Although it has been a well-known property of graphene, some previous open Z-scan experiments of graphene have not observed SA phenomenon, either[12, 31-33]. The reason might come from the experiment condition, sample concentration, and the quality of graphene. The fitted 2PA coefficient of pure graphene is 0.59 and 0.40 cm/GW at 1064 and 532 nm, which are smaller than the values of N-Gns (0.76, 0.46 cm/GW). As demonstrated in the inset of figure 7, the doping of N atoms in graphene opens the zero band gap and decreases the energy band volume[21], corresponding the threshold of nonlinear absorption is reduced. The experiment proves the superiority of N-Gns for NLO applications.

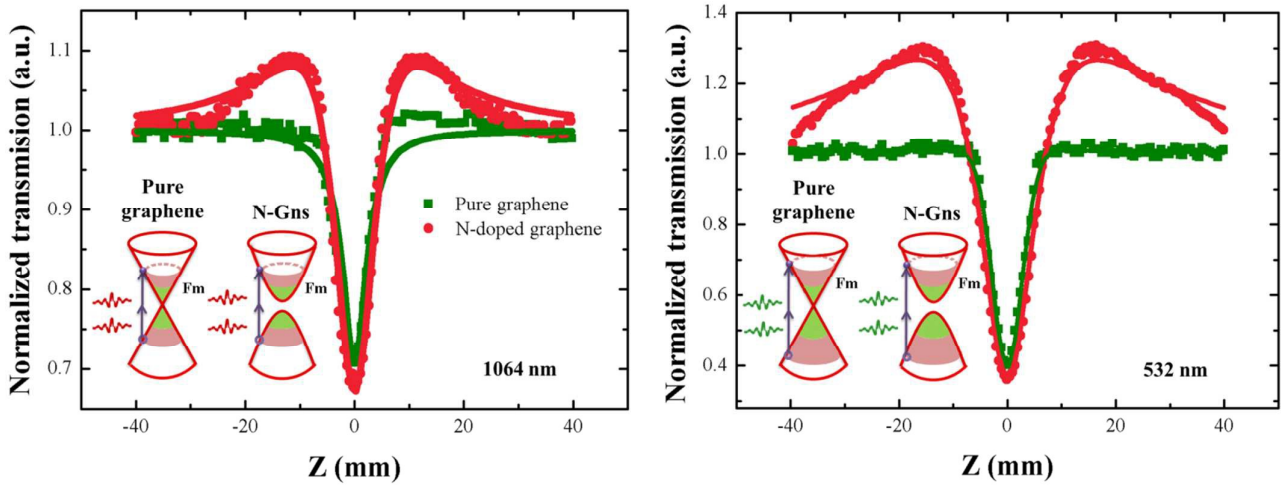

Figure 7 Nonlinear transmissions of pure graphene and N-Gns under the same energy excitations of 6 μJ at 1064nm (left) and 12 μJ at 532 nm (right). (The points are the experimental data, and the solid lines are the fitted curves). Insert: schematic diagram for the energy level transitions of pure graphene and N-Gns.

The imaginary part of the third-order NLO susceptibility, $\mathrm{Im}\chi^{(3)}$, is directly related to the 2PA coefficient β. Their relationship can be expressed as

$$\mathrm{Im}\,\chi^{(3)} = \frac{c^2 n_0^2}{240 * \pi^2 \omega}\beta(m/W) \quad (5)$$

where c is the light speed in vacuum, n_0 is the linear refractive index and ω is the angular frequency of the excitation light. The figure of merit (FOM) for the third-order optical nonlinearity is defined as FOM = $|\mathrm{Im}\chi^{(3)}/\alpha_0|$. Referencing above results, $\mathrm{Im}\chi^{(3)}$ and FOM of N-Gns are calculated to be 1.30×10^{16} $m^3(sW)^{-1}$, 5.8×10^{13} $m^4(sW)^{-1}$ for 1064 excitation, and 1.57×10^{16} $m^3(sW)^{-1}$, 7.0×10^{13} $m^4(sW)^{-1}$ for 532 nm excitation, respectively.

Conclusion.

For N-Gns which consist of 1~5 atomic layers, the XPS measurement confirms the existence of N atoms, which exhibits three different bond structures. An open-aperture Z-scan equipment is adopted to detect the NLO properties, including SA and OL effects at different excitation wavelengths and energies. By comparison, the NLO characteristic of N-Gns is proved to be superior to that of pure graphene. It indicates that the N-Gns will be a good substitute to the pure graphene in optoelectronic field, especially for NLO applications.

Acknowledgements

This work was supported by the National Natural Science Foundation of China (Grant No. 61178060), and Natural Science Foundation for Distinguished Young Scholar of Shandong Province (2012JQ18).

Notes and references

1 R. R. Nair, P. Blake, A. N. Grigorenko, K. S. Novoselov, T. J. Booth, T. Stauber, N. M. R. Peres and A. K. Geim, *Science*, 2008, 320, 1308.
2 Z. H. Ni, H. M. Wang, J. Kasim, H. M. Fan, T. Yu, Y. H. Wu, Y. P. Feng and Z. X. Shen, *NanoLett*., 2007 7 (9), 2758-2763 ().
3 X. Du, I. Skachko, A. Barker and E. Y. Andrei, *Nat. Nano*., 2008, 3, 491.
4 K. S. Kim, Y. Zhao, H. Jang, S. Y. Lee, J. M. Kim, K. S. Kim, J. H. Ahn, P. Kim, J. Y. Choi and B. H. Hong, *Nature*, 2009, 457, 706.
5 A. A. Balandin, S. Ghosh, W. Z. Bao, I. Calizo, D. Teweldebrhan, F. Miao and C. N. Lau, *NanoLett.*, 2008, 8, 902.
6 K. S. Novoselov, A. K. Geim, S. V. Morozov, D. Jiang, Y. Zhang, S. V. Dubonos, I. V. Grigorieva and A. A. Firsov, *Science*, 2004, 306, 666.
7 J. M. B. Lopes dos Santos, N. M. R. Peres and A. H. Castro Neto, *Phys. Rev. Lett.,* 2007, 99, 256802.
8 A. B. Kuzmenko, E. van Heumen, F. Carbone and D. van der Marel, *Phys. Rev. Lett.*, 2008, 100, 117401.
9 F. Bonaccorso, Z. Sun, T. Hasan and A. C. Ferrari, *Nature Photonics*, 2010, 4, 611.
10 A. R. Wright, X. G. Xu, J. C. Cao and C. Zhang, *Appl. Phys. Lett.*, 2009, 95, 072101.
11 J. Wang, Y. Hernandez, M. Lotya, J. N. Coleman and W. J. Blau, *Adv. Mater.*, 2009, 21, 2430.
12 M. Feng, H. B. Zhan and Yu Chen, *Appl. Phys. Lett.*, 2010, 96, 033107.
13 Z. W. Zheng, C. J. Zhao, S. B. Lu, Yu Chen, Y. Li, H. Zhang and S. C. Wen, *Opt. Express*, 2012, 20, 23201.
14 F. Zhang, S. Han, Y. Liu, Z. P. Wang and X. G. Xu, *Appl. Phys. Lett.*, 2015, 106, 091102.
15 Q. L. Bao, H. Zhang, Y. Wang, Z. H. Ni, Y. L. Yan, Z. X. Shen, K. P. Loh and D. Y. Tang, *Adv. Funct. Mater.*, 2009, 19, 3077.
16 J. Ma, G. Q. Xie, P. Lv, W. Gao, P. Yuan, L. Qian, U. Griebner, V. Petrov, H. Yu, H. Zhang and J. Wang, *Scientific Reports*, 2014, 4, 1.
17 S. Husaini, J. E. Slagle, J. M. Murray, S. Guha, L. P. Gonzalez and R. G. Bedford, *Appl. Phys. Lett.*, 2013, 102, 191112.

18 Q. Y. Ouyang, Z. Xu, Z. Y. Lei, H. W. Dong, H. L. Yu, L. H. Qi, C. Y. Li and Y. J. Chen, *Carbon*, 2014, 67, 214.
19 G. S. Kumar, R. Roy, D. Sen, U. K. Ghorai, R. Thapa, N. Mazumder, S. Sahab and K. K. Chattopadhyay, *Nanoscale*, 2014, 6, 3384.
20 M. B. Krishna, V. P. Kumar, N. Venkatramaiah, R. Venkatesan and D. N. Rao, *Appl. Phys. Lett.*, 2011, 98, 081106.
21 D. C. Wei, Y. Q. Liu, Y. Wang, H. L. Zhang, L. P. Huang and G. Yu, *Nano Lett.*, 2009, 9, 1752.
22 K. S. Kim, Y. Zhao, H. Jang, S. Y. Lee, J. M. Kim, K. S. Kim, J. Ahn, P. Kim, J. Choi and B. H. Hong, *Nature*, 2009, 457, 706.
23 A. Reina, X. T. Jia, J. Ho, D. Nezich, H. Son, V. Bulovic, M. S. Dresselhaus and J. Kong, Large Area, *Nano Lett.*, 2009, 9, 30.
24 F. Han, S. M. Yang, W. X. Jing, Z. D. Jiang, H. Liu and Lei Li, *Appl. Surf. Sci.*, 2015, 345, 18.
25 B. Anand, R. Podila, A. M. Rao, R.i Philip, S. Sai, *AIP Conf. Proc.,* 2013, 1536, 735.
26 N. K. M. Naga Srinivas, S. Venugopal Rao and D. Narayana Rao, *J. Opt. Soc. Am. B*, 2003, 20, 2470.
27 H. Zhan, Z. G. Zhou, J. L. He and A. X. Lin, *Opt. Lett.*, 2012, 37, 3408.
28 L. Wang, H. T. Huang, D. Y. Shen, J. Zhang, H. Chen, Y. Wang, X. Liu and D. Y. Tang, *Opt. Express*, 2014, 22, 19495.
29 B. S. Kalanoor, P. B. Bisht, S. A. Ali, T. T. Baby and S. Ramaprabhu, *J. Opt. Soc. Am. B*, 2012, 29, 669.
30 J. L. Wu, B. Gu, N. Sheng, D. H. Liu and Y. P. Cui, *Appl. Phys. Lett.*, 2014, 105, 171113.
31 J. Wang, Y. Hernandez, M. Lotya, J. N. Coleman and W. J. Blau, *Adv. Mater.*, 2009, 21, 2430.
32 L. Yan, Y. Xiong, J. Si, X. Sun, W. Yi and X. Hou, *Opt. Express*, 2014, 22, 31836.
33 B. Anand, A. Kaniyoor, S. S. Sai, R. Philipc and S. Ramaprabhu, *J. Mater. Chem. C*, 2013, 1, 2773.